

Elastic and charge transfer processes in $H^{++}CO$ collisions

T. J. Dhillip Kumar, A. Saieswari, and Sanjay Kumar

Citation: *J. Chem. Phys.* **124**, 034314 (2006); doi: 10.1063/1.2158998

View online: <http://dx.doi.org/10.1063/1.2158998>

View Table of Contents: <http://jcp.aip.org/resource/1/JCPSA6/v124/i3>

Published by the [American Institute of Physics](#).

Additional information on *J. Chem. Phys.*

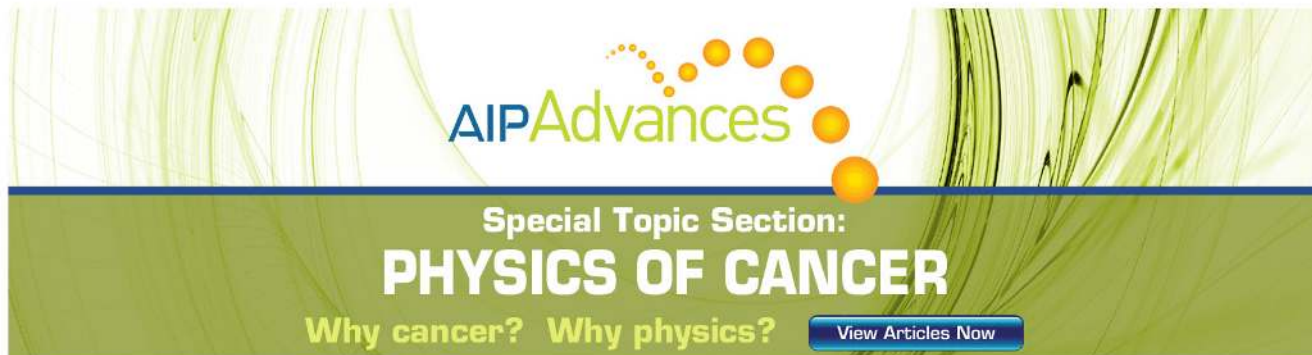
Journal Homepage: <http://jcp.aip.org/>

Journal Information: http://jcp.aip.org/about/about_the_journal

Top downloads: http://jcp.aip.org/features/most_downloaded

Information for Authors: <http://jcp.aip.org/authors>

ADVERTISEMENT



AIP Advances

Special Topic Section:
PHYSICS OF CANCER

Why cancer? Why physics? [View Articles Now](#)

Elastic and charge transfer processes in $H^+ + CO$ collisions

T. J. Dhilip Kumar, A. Saieswari, and Sanjay Kumar^{a)}

Department of Chemistry, Indian Institute of Technology, Madras, Chennai 600 036, India

(Received 26 September 2005; accepted 29 November 2005; published online 20 January 2006)

Proton and hydrogen atom time-of-flight spectra in collision energy range of $E_{\text{trans}}=9.5\text{--}30$ eV show that the endoergic charge transfer process in the $H^+ + CO$ system is almost an order of magnitude less probable than the elastic scattering [G. Niedner-Schatteburg and J. P. Toennies, *Adv. Chem. Phys.* **LXXXII**, 553 (1992)]. *Ab initio* computations at the multireference configuration interaction level have been performed to obtain the ground- and several low-lying excited electronic state potential energy curves in three different molecular orientations namely, H^+ approaching the O-end and the C-end (collinear), and H^+ approaching the CO molecule in perpendicular configuration with fixed CO internuclear distance. Nonadiabatic coupling terms between the ground electronic state ($H^+ + CO$) and the three low-lying excited electronic states ($H + CO^+$) have been computed and the corresponding diabatic potentials have been obtained. A time-dependent wavepacket dynamics study is modeled first involving only the ground and the first excited states and then involving the ground and the three lowest excited states at the collision energy of 9.5 eV. The overall charge transfer probability have been found to be $\approx 20\% - 30\%$ which is in qualitative agreement with the experimental findings. © 2006 American Institute of Physics.

[DOI: 10.1063/1.2158998]

I. INTRODUCTION

Proton interaction with simple molecules is of fundamental importance in several areas of molecular physics and astrophysics. For example, the solar flare consists of mainly protons, which enter the earth's ionosphere with mean kinetic energy (KE) 1 to 2 KeV.¹ These protons lose most of their KE by various inelastic processes, and finally reach the region of the stratosphere interacting with many diatomic and polyatomic molecules with KE in the range of 0–100 eV. As a result, proton-molecule interaction has been the subject of many experimental and theoretical studies, and a wealth of varied experimental information on vibrationally rotationally inelastic collisions with the diatomic and polyatomic molecules has become available over the years using molecular beams and proton energy-loss spectroscopic techniques.^{2–6} On the other hand, proton-molecule reactions play a central role in the interstellar clouds. Protonated bound molecular species such as H_3^+ , N_2H^+ , HCO^+ , HOC^+ , and HCS^+ have been identified in the interstellar media through radio-astronomical spectra.⁷

The focus has been on collision energies (E_{trans}) between 0 and 30 eV where extensive vibrational-rotational excitations of target molecules are expected to occur along with charge transfer (CT) collisions. Experimentally, it has been observed that there is a marked selectivity for vibrational excitations (vibrational inelasticity) in apparently similar molecules. For example, in this E_{trans} range the amount of vibrational excitation in N_2 , CO , and NO with the collision of H^+ is very low while it is larger in H_2 , and it is even larger in O_2 . The $H^+ + CO$ system has been investigated by Krutein and Linder³ and the energy loss spectra show a very low

vibrational inelasticity. The broadening of the energy loss peaks has been attributed to the rotational excitations taking place in the system. Better resolved proton and hydrogen atom time-of-flight spectra for the $H^+ + CO$ system confirmed the small probabilities of about 10% for $v=1$ excitation.^{4,8}

Proton-molecule interactions operate over a wide range of distance. For example, even when a proton is at a large distance from a molecule it can interact with the molecule through the long-range tail of the interaction potential. At shorter distances valence forces dominate the interactions. Since the proton lacks the structural electronic features, it interacts strongly with the target electronic cloud by deforming the overall charge distribution of the molecule. As a result, quite often the low-lying excited electronic potential energy surfaces (PES) interact with the ground electronic state (GS) PES, thus influencing the overall energy transfer processes.

In the $H^+ + H_2$ system, there is an avoided crossing between the GS PES and the next higher PES which asymptotically corresponds to the $H + H_2^+$, giving rise to the CT process. In the $H^+ + O_2$ system, there is a direct curve crossing between the GS PES and the first excited state PES corresponding to the $H + O_2^+$. For details see Ref. 4 and references therein. Interestingly, in the $H^+ + N_2$ system, the low-lying excited state PESs are found to be well separated energetically from the GS PES.⁹ Exact quantum dynamical calculations for vibrational excitation processes in the vibrational close-coupling rotational infinite-order sudden approximation (VCC-RIOS) framework^{6,10} have been performed using *ab initio* PESs for the $H^+ + H_2$ system¹¹ and the $H^+ + N_2$ system,⁹ and employing semiempirical *diatomics in molecules* (DIM) PESs for the $H^+ + O_2$ system.¹² The three-dimensional quantum mechanical calculations for the reac-

^{a)}Electronic address: sanjay@iit.ac.in

tive and the CT collisions have also been carried out within the coupled states approximation for the $H^+ + H_2$ system,¹³ and using the close-coupling formalism with hyperspherical coordinates for the $D^+ + H_2$ system.¹⁴ Using the latter approach the details of quantum dynamics of the reactive and the CT has been analyzed recently for the $H^+ + H_2$ system.¹⁵

There have been many theoretical studies (see Ref. 16 and references therein) on the $H^+ + CO$ system where the focus has been on the characterization of the GS potential well. In recent years, high level *ab initio* computations have become available characterizing the interaction well. Puzzarini *et al.*¹⁷ computed the GS PES of HCO^+ ion near its equilibrium geometry (collinear) and predicted the vibrational and rotational frequencies of the HCO^+ ion using variational calculations at the CASSCF-MRCI/*cc-pVQZ* level of theory. Mladenovic and Schmatz computed the three-dimensional ground state PES for the $HCO^+ - HOC^+$ ions using the CCSD(T) method employing the *cc-pVQZ* basis set of Dunning, and predicted the rovibrational spectrum along with the number and densities of bound vibrational states.¹⁸ Just recently, a new full three-dimensional GS PES in Jacobi coordinates was obtained by our group¹⁶ to study the time-independent quantum dynamics of vibrational excitations in the system in the framework of VCC-RIOSAscheme on the GS PES. Overall, the computed collision attributes were found to be in good agreement with the experiments.

The asymptotic CT channel, $H + CO^+$ is endoergic (≈ 0.42 eV) as compared to the asymptotic $H^+ + CO$ channel.⁴ Therefore, it is expected that probability of the CT processes would be less, and that they would be accessible only by the Rosen-Zener-Demkov-type of coupling.¹⁹ This is confirmed by the experimentally observed^{4,5} total differential cross section (DCS) for proton and H-atom detection in the $H^+ + CO$ scattering at $E_{lab} = 30$ eV where the CT was found to be almost an order of magnitude less probable than the elastic scattering and the vibrational excitations.

In a recent study, the CT dynamics (electron capture) has been studied in the system at very high collision energies ($E_{coll} = 10$ KeV/u) by Kimura *et al.*²⁰ They computed the GS as well as the first and the second excited state potential energy curves (PEC) (CO fixed at its equilibrium geometry, r_{eq}) for the collinear and the perpendicular approaches of H^+ using the MRCI method employing the *cc-pVTZ* basis. They also computed electron capture cross section and DCS for these molecular orientations along with averaged DCS and compared with the experimental results of Gao *et al.*^{20,21} at E_{coll} of 1.5 KeV/u.

The focus of the present study is to examine the role of the low-lying excited states in influencing the overall dynamics of the $H^+ + CO$ collisions relevant to proton energy-loss experiments in the energy range $E_{trans} = 9.5 - 30$ eV. The probability of the charge transfer collisions at $E_{lab} = 30$ eV is estimated to be an order of magnitude less ($\approx 10\%$) as compared to that of total elastic collisions.⁴ Since the experiments show little amount of vibrational excitations ($v = 0 \rightarrow v' = 1$) we analyze the behavior of PECs with CO internuclear distance r fixed at its equilibrium value (r_{eq}) for the collinear as well as perpendicular approaches of H^+ , and ex-

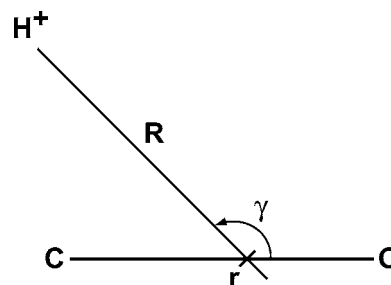


FIG. 1. Jacobi coordinates.

amine the dynamics at $E_{trans} = 9.5$ eV ($E_{lab} = 9.8$ eV). We first assume that only the ground- and the first excited states are largely involved due to the coupling between the two-states in influencing the collision dynamics in Sec. III. Nevertheless, the influence of the other low-lying excited states cannot be ruled out and the extent of their involvement relevant to experimental proton-energy loss experiments at $E_{lab} = 9.8$ eV is discussed in Sec. IV where four electronic states are coupled. A time-dependent wavepacket study is undertaken to model and estimate the probabilities for the total elastic and the CT dynamics in the two cases.

The present paper is organized as follows. In Sec. II we describe the details of computations for the adiabatic PECs and the nonadiabatic coupling matrix elements along with the corresponding diabatic potentials and mixing angles. A model time-dependent quantum dynamics is studied involving only the two diabatic curves in Sec. III, and involving the four diabatic curves in Sec. IV, followed by summary and conclusions in Sec. V.

II. COMPUTATIONAL METHODOLOGY

A. *Ab initio* adiabatic potential energy curves

Ab initio calculations have been performed in the Jacobi coordinates (Fig. 1) where R is the H^+ distance from the center of mass of CO, r is the interatomic distance of CO, and $\gamma = \cos^{-1}(R.r)$. The calculations have been carried out in three different molecular orientations, i.e., (i) H^+ approaching the oxygen atom in the collinear configuration, ($\gamma = 0^\circ$), (ii) H^+ approaching the center of mass of the CO molecule in the perpendicular configuration, ($\gamma = 90^\circ$), and (iii) H^+ approaching the carbon atom in the collinear configuration, ($\gamma = 180^\circ$). The calculations have been performed in C_{2v} and C_s point groups for the collinear and perpendicular approaches, respectively. PECs as a function of R have been obtained for the three molecular orientations with the set of grid points: $R = 1.4 - 2.4(0.2)$, $2.4 - 3.8(0.1)$, $3.8 - 5.0(0.2)$, $5.0 - 7.0(0.4)$, and $7.0 - 20.0(1.0)$ a_0 for the collinear approaches, and $R = 1.0 - 2.4(0.2)$, $2.4 - 3.8(0.1)$, $3.8 - 5.0(0.2)$, $5.0 - 7.0(0.4)$, and $7.0 - 20.0(1.0)$ a_0 for the perpendicular orientation. The numbers in parentheses indicate the increments in the stated intervals. The adiabatic curves of the ground and the low-lying excited singlet states are obtained by the multireference configuration interaction (MRCI) method using the MOLPRO suite of programs.²² We have used Dunning's *cc-pVTZ* basis sets for H, C, and O atoms.²³ The

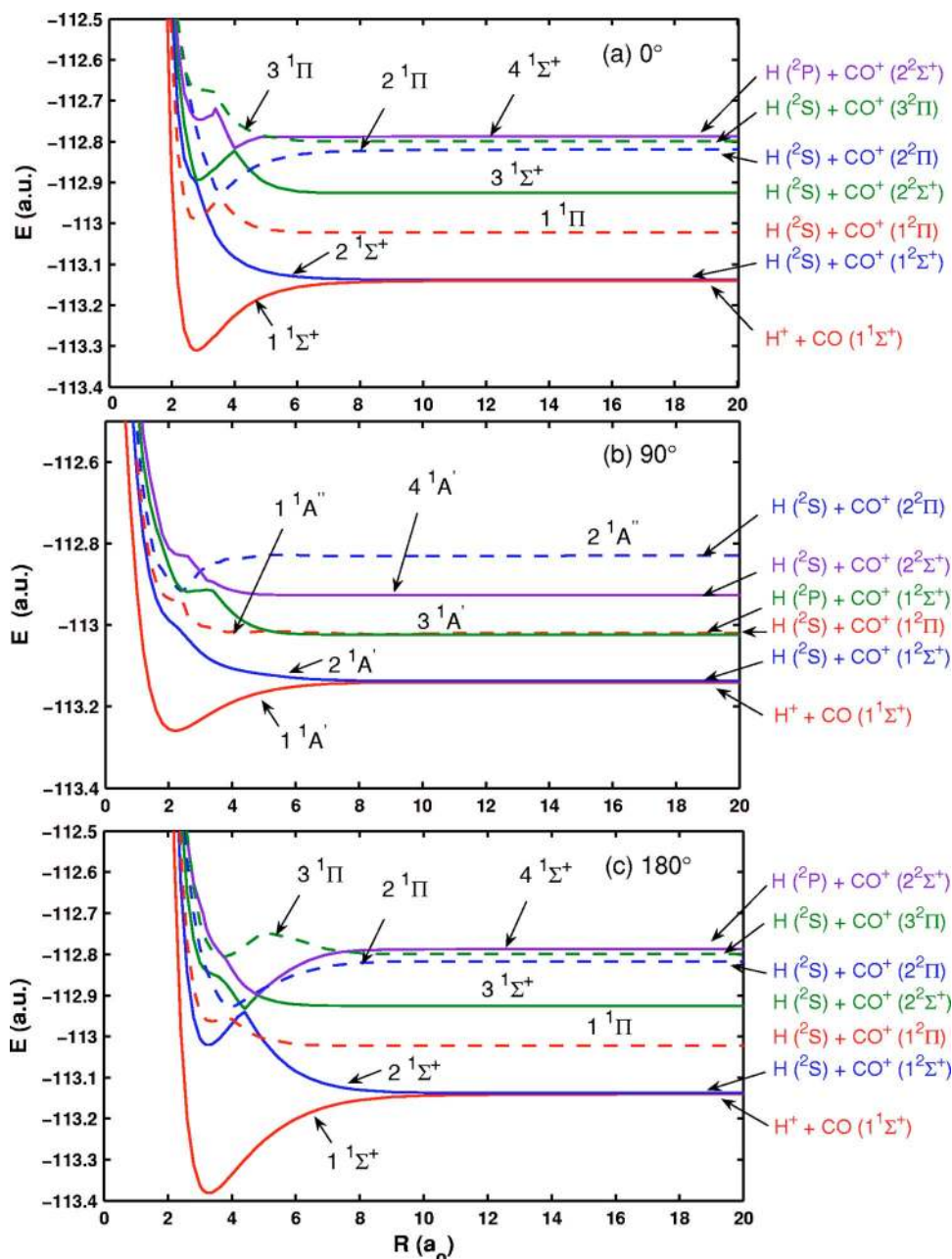


FIG. 2. Adiabatic potential energy curves for $\gamma=0^\circ$, 90° , and 180° molecular orientations. The $1^1\Sigma^+$ and the $1^1A'$ curves are shown with solid lines while the $1^1\Pi$ and the $1^1A''$ curves are shown as dashed curves.

adiabatic PECs for the three different molecular orientations $\gamma=0^\circ$, 90° , and 180° are shown in Fig. 2. For the collinear orientations the 1–4 $1^1\Sigma^+$ and the 1–3 $1^1\Pi$ states have been computed and in the perpendicular orientation, the 1–4 $1^1A'$ and the 1,2 $1^1A''$ states have been obtained. The $1^1\Sigma^+$ state corresponds to the entrance channel, $H^+ + CO(1^1\Sigma^+)$, whereas the $2^1\Sigma^+$ state corresponds to the CT channel, $H(2S) + CO^+(1^2\Sigma^+)$, in the collinear geometries. The $1^1A'$ state corresponds to the entrance channel, $H^+ + CO(1^1\Sigma^+)$, whereas the $2^1A'$ state corresponds to the CT channel, $H(2S) + CO^+(1^2\Sigma^+)$, in the perpendicular geometry.

For the sake of clarity, in Fig. 3, we have magnified the curves in the interaction region except for the GS curve. For $\gamma=0^\circ$ and $\gamma=180^\circ$, the $2^1\Sigma^+$ state has an avoided crossing with the $3^1\Sigma^+$ state near $R=2.8$ and 4.4 a., respectively, while the $3^1\Sigma^+$ state shows an avoided crossing with the $4^1\Sigma^+$ state near $R=4.0$ and 4.8 a., respectively. Again, as we

can see in Fig. 3, for $\gamma=0^\circ$, the $4^1\Sigma^+$ has an avoided crossing with its higher state near $R=3.4$ a., which appears to be not so pronounced for $\gamma=180^\circ$. The $1^1\Pi$ state also exhibits an avoided crossing with the $2^1\Pi$ state near $R=3.6$ and 3.8 a., for $\gamma=0^\circ$ and $\gamma=180^\circ$, respectively. For $\gamma=90^\circ$, an avoided crossing is seen between the $3^1A'$ and the $4^1A'$ states near $R=3.2$ a., and the $1^1A''$ and the $2^1A''$ near $R=2.4$ a. A typical Rosen-Zener-Demkov type of coupling^{19,24,36} is seen between the ground and the first excited states in all the three orientations and between the $2^1\Pi$ and the $3^1\Pi$ states in the collinear orientations. The energy difference between the asymptotic channels, $H^+ + CO(1^1\Sigma^+)$ and $H(2S) + CO^+$, is found to be 0.39 eV as compared to the reported experimental value of 0.42 eV.⁴ The nature of the curves confirms that the system is rich in nonadiabatic dynamics and at higher energy collisions such effects become important for energy transfer mechanism. For

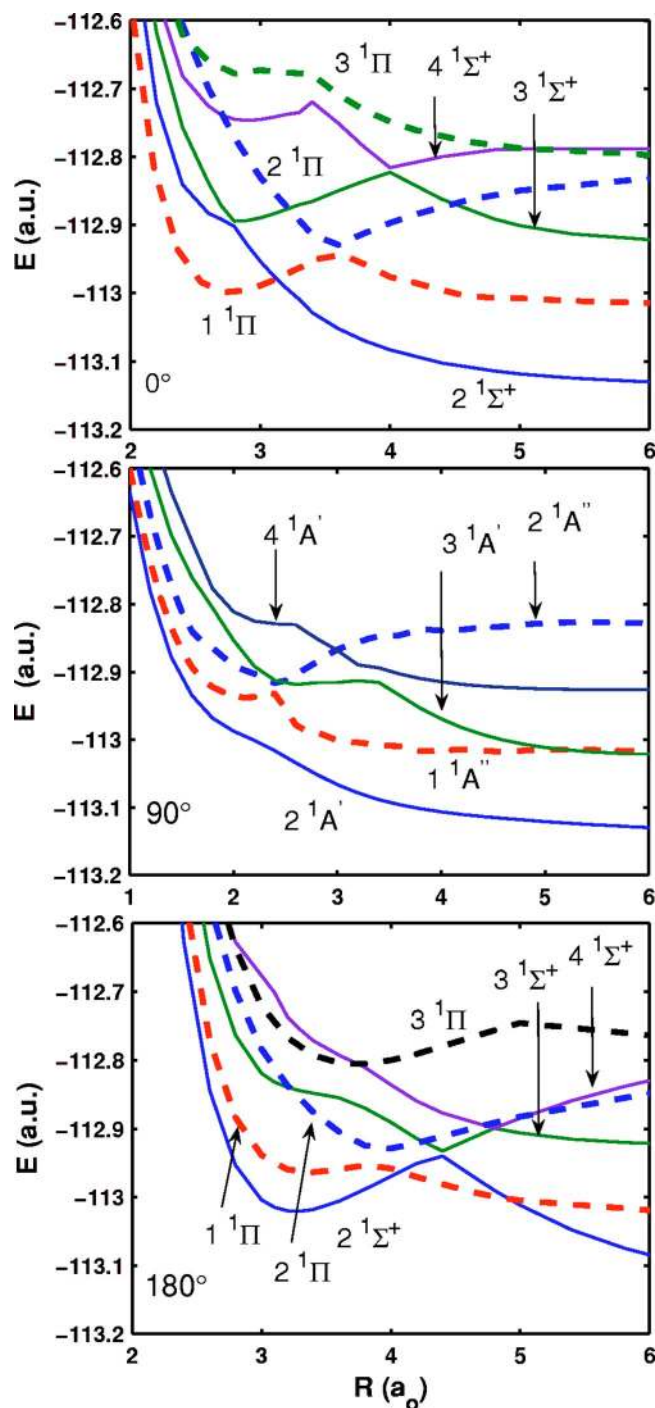


FIG. 3. Same as in Fig. 2 but on the magnified scale in the interaction region. The ground states $1^1\Sigma^+$ and $1^1A'$ are not shown.

dynamics calculation we focus below on the PECs for the $1^1\Sigma^+$ symmetry in the collinear approaches and the $1^1A'$ symmetry in the perpendicular approach.

B. Nonadiabatic coupling matrix elements

For the present study, the dynamical calculations in the adiabatic representation requires a knowledge of the kinetic coupling elements of the form

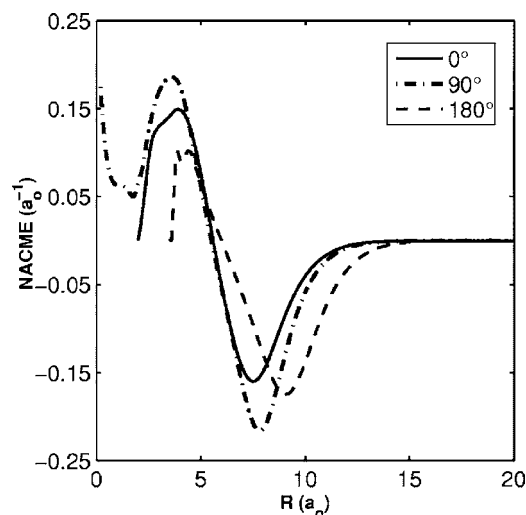


FIG. 4. Radial nonadiabatic coupling matrix elements (NACME) for the ground and the first excited states for three molecular orientations.

$$\tau = \langle \psi_1^e | \frac{d^n}{dR^n} | \psi_2^e \rangle, \quad (1)$$

where $n=1$ or 2 . The terms with $n=2$ are generally neglected since they are generally small in magnitude.²⁵ The kets $|\psi_1^e\rangle$ and $|\psi_2^e\rangle$ represent the electronic wave functions of the two adiabatic states and R stands for the radial nuclear coordinate. Nonadiabatic coupling matrix elements (NACME) have been computed between the GS and the first excited states by numerical differentiation using finite difference method²⁶

$$\langle \psi_1^e | \frac{d^n}{dR^n} | \psi_2^e \rangle_{R_0} = \frac{1}{2\Delta R} \langle \psi_1^e(R_0 + \Delta R) | \psi_2^e(R_0 - \Delta R) \rangle \quad (2)$$

where ΔR is the small increment. We have used the MOLPRO code²² to compute the NACME values. In this procedure, first the orbitals are determined at the reference geometry, then the calculations are performed at the displaced geometries. The NACME values have been obtained using the MRCI method by computing the finite-differences of configuration interaction (CI) wave functions with ΔR of $0.0002 a_0$. Additional calculations were also performed for a few data points with $\Delta R=0.002 a_0$, and the obtained values were identical with the values obtained with $\Delta R=0.0002 a_0$. In earlier nonadiabatic studies for He–CN collisions²⁷ and for H_2S photodissociation,^{28,29} NACME values were also computed using the MOLPRO software with similar increment in ΔR .

The NACME values are plotted as a function of R in Fig. 4 for all three molecular orientations. Kimura *et al.*²⁰ had computed the NACME values for this system and our results compare well with their data. Generally, for all the three orientations, couplings show similarities in shape. In the case of H^+ approaching the C atom in the collinear geometry ($\gamma = 180^\circ$), the minimum position is found to be farther out at $R=9.1 a_0$.

C. Diabatization—mixing angle

For the computational convenience we treat the coupling between the two and the four electronic states in a diabatic

representation. The diabaticization procedures, their exactness and their associated advantages for numerical computations have been discussed and documented in the literature in detail.^{25,30–43} A general discussion on it has also been recently published.⁴¹ For the convenience and familiarity of terms, we summarize the essential details below.

For a two-state coupling, the transformation from an adiabatic representation, with electronic wave functions $\psi_{1,2}^a$, to a diabatic representation characterized by electronic wave functions $\psi_{1,2}^d$, is achieved by a unitary transformation

$$\begin{pmatrix} \psi_1^d \\ \psi_2^d \end{pmatrix} = \begin{pmatrix} \cos \alpha & \sin \alpha \\ -\sin \alpha & \cos \alpha \end{pmatrix} \begin{pmatrix} \psi_1^a \\ \psi_2^a \end{pmatrix}, \quad (3)$$

where α is the mixing angle describing the mixing between the two adiabatic electronic states and it is a function of R . Since $\langle \psi_1^d | d/dR | \psi_2^d \rangle \approx 0$, the mixing angle α can be obtained by integration of NACME,^{26,27,29,31}

$$\alpha(R) = \alpha_{R_{\text{ref}}} + \int_{R_{\text{ref}}}^R \langle \psi_1^a | \frac{d}{dR'} | \psi_2^a \rangle dR', \quad (4)$$

where $\alpha_{R_{\text{ref}}}$ is chosen to be zero at $R=R_{\text{ref}}$, assuming that the adiabatic and diabatic representations become identical at R_{ref} .

Using the Eq. (3), the matrix elements of \hat{H}_{el} is given by,

$$V_{11}^d = \langle \psi_1^d | \hat{H}_{el} | \psi_1^d \rangle = V_1^a \cos^2 \alpha + V_2^a \sin^2 \alpha, \quad (5)$$

$$V_{22}^d = \langle \psi_2^d | \hat{H}_{el} | \psi_2^d \rangle = V_1^a \sin^2 \alpha + V_2^a \cos^2 \alpha, \quad (6)$$

$$V_{12}^d = \langle \psi_1^d | \hat{H}_{el} | \psi_2^d \rangle = (V_1^a - V_2^a) \cos \alpha \sin \alpha, \quad (7)$$

and $V_{12}^d = V_{21}^d$. The $V_{1,2}^a$ are the potential energies in the adiabatic representation. V_{11}^d and V_{22}^d are the corresponding potentials in the diabatic representation, and V_{12}^d is the coupling potential between the two-states.

Several authors have proposed schemes to derive α from the knowledge of NACME obtained from the solution of electronic Schrödinger equation.^{44,45} Other approximate methods^{26,27,46–48} have also been suggested which avoid the direct computation of NACME and α is obtained from the CI coefficients of the electronic wave functions.

In the present study we have used the MOLPRO code to obtain the quasi-diabatic states directly wherein the diabaticization is achieved by determining the diabatic wave functions and the corresponding CI vectors which vary as little as possible as a function of geometry.^{26,27,47} This condition is met by using the invariance of the MRCI energies with respect to unitary transformations among the active orbitals so that the geometry dependence of the orbitals is minimized. This is accomplished by maximizing the overlap for all the pairs of active orbitals at R_{ref} with those at a neighbourhood geometry R' using the Jacobi rotation technique. The description and application of the procedure for a general case is described in detail in Ref. 29.

For the two-state coupling model involving the $1^1\Sigma^+(1^1A')$ and the $2^1\Sigma^+(2^1A')$ states, we computed the diabatic potentials directly from the MOLPRO software. We also computed NACME values as a function of R and deter-

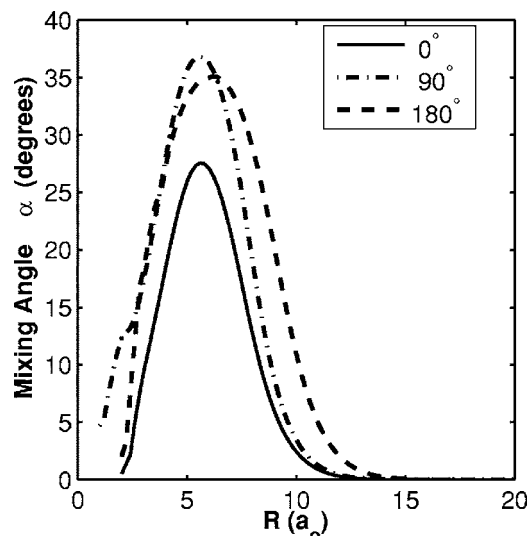


FIG. 5. Mixing angle α obtained between the ground and the first excited states for three molecular orientations.

mined the mixing angle using Eq. (4) with $R_{\text{ref}}=16$ a₀. The obtained mixing angle α is shown as a function of R in Fig. 5. It can be seen that α goes to zero for $R \geq 16$ a₀, for which both the adiabatic and the diabatic representations are assumed to be identical. We also obtained the diabatic potentials from the computed α values using Eqs. (5)–(7) which were found to be identical with those obtained directly from the MOLPRO computations. In Fig. 6 diabatic potentials, (V_{11}^d and V_{22}^d , shown in dashed lines) and the corresponding adiabatic potentials, (V_1^a and V_2^a , shown in full lines) obtained from the MOLPRO code are shown for all the three orientations. It is important to point out here that the two adiabatic PECs shown in Fig. 6 show Rosen-Zener-Demkov type of coupling¹⁹ exhibiting wide regions of weakly coupled and nearly parallel adiabatic PECs. In such situations the diabatic PECs do not cross. This has also been found for other model systems exhibiting this type of coupling.³⁸

For the four-state coupling involving $1-4^1\Sigma^+$ states for $\gamma=180^\circ$ we have again obtained the 4×4 diabatic potential matrix directly using the MOLPRO software, and we discuss the results for this case in Sec. IV.

III. TWO-STATE COUPLING DYNAMICS

In this section we model the two-state coupling dynamics in terms of time-dependent wavepacket (TDWP) propagation. The TDWP method⁴⁹ involves the following steps: (1) Preparing the initial wavepacket (WP) on a finite grid; (2) propagating the WP until the end of the dynamical event, and (3) analyzing the final WP for reaction attributes in the asymptotic regions.

For the two-state coupled system, the time-dependent Schrödinger equation for the nuclear motion in the adiabatic representation is

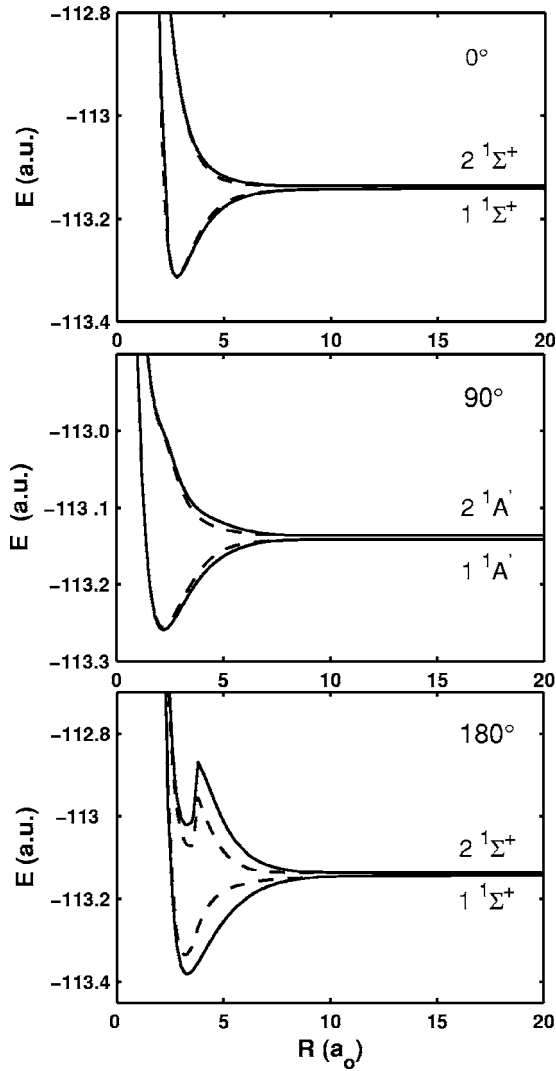


FIG. 6. Adiabatic and diabatic potential energy curves for $\gamma=0^\circ$, 90° , and 180° . Full lines indicate adiabatic curves and dashed lines indicate diabatic curves.

$$i\hbar \frac{\partial}{\partial t} \begin{pmatrix} \psi_1(t) \\ \psi_2(t) \end{pmatrix} = \begin{bmatrix} -\frac{\hbar^2}{2\mu} (\nabla^2 + \hat{T}_{11}) & \hat{T}_{12} \\ \hat{T}_{21} & \nabla^2 + \hat{T}_{22} \end{bmatrix} \begin{pmatrix} \psi_1(t) \\ \psi_2(t) \end{pmatrix} + \begin{pmatrix} V_1^a & 0 \\ 0 & V_2^a \end{pmatrix} \begin{pmatrix} \psi_1(t) \\ \psi_2(t) \end{pmatrix}, \quad (8)$$

where $\hat{T}_{11} = \langle \psi_1^a | \nabla_R^2 | \psi_1^a \rangle$,

$$\hat{T}_{12} = \hat{T}_{21} = \langle \psi_1^a | \nabla_R^2 | \psi_2^a \rangle + 2 \langle \psi_1^a | \nabla_R | \psi_2^a \rangle \cdot \nabla_R, \text{ and}$$

$$\hat{T}_{22} = \langle \psi_2^a | \nabla_R^2 | \psi_2^a \rangle.$$

$\psi_{1(2)}$ are the nuclear wave functions for the states 1(2).

In the diabatic representation the time-dependent Schrödinger equation for the nuclear motion is given as

$$i\hbar \frac{\partial}{\partial t} \begin{pmatrix} \psi_1(t) \\ \psi_2(t) \end{pmatrix} = \left[\begin{pmatrix} \hat{T}_1 & 0 \\ 0 & \hat{T}_2 \end{pmatrix} + \begin{pmatrix} V_{11}^d & V_{12}^d \\ V_{12}^d & V_{22}^d \end{pmatrix} \right] \begin{pmatrix} \psi_1(t) \\ \psi_2(t) \end{pmatrix}, \quad (9)$$

where \hat{T}_1, \hat{T}_2 are kinetic energy operators of the nuclear motions on the respective diabatic states and V_{11}^d, V_{22}^d , and V_{12}^d

are diabatic potentials. If the diabatic coupling potential V_{12}^d is zero, then the two wavepackets would propagate independently of each other on the respective diabatic PECs.

The time-evolution of the nuclear WP is governed by

$$\psi(t) = \hat{U}(t, t_0) \psi(t_0). \quad (10)$$

where $\hat{U}(t, t_0)$ is the time-evolution operator. For an explicitly time-independent Hamiltonian operator \hat{H}

$$\hat{U}(t, t_0) = \exp(-i\hat{H}(t - t_0)/\hbar). \quad (11)$$

The initial WP, ψ_1 , is prepared in the asymptotic region ($\text{H}^+ + \text{CO}(1^1\Sigma^+)$ channel) at $R=12$ a, where it is assumed that there is no influence of the long-range asymptotic potential. We have chosen a minimum uncertainty Gaussian wavepacket (GWP)⁵⁰ of the form:

$$\psi(R, t=0) = (2\pi\delta)^{-1/4} \exp\left(-\frac{(R-R_0)^2}{4\delta^2} - ik_0R\right), \quad (12)$$

where δ is the width parameter of the GWP, and R_0 and k_0 are its locations in the coordinate and momentum space, respectively, and $k_0 = \sqrt{2\mu E}/\hbar$. The radial kinetic-energy operator is evaluated using the fast Fourier transform (FFT) method.⁵¹ The Chebychev polynomial expansion method⁵² is chosen for the WP propagation since the system exhibits long time dynamics. In this scheme, the evolution operator \hat{U} is approximated in the Chebychev series. Since the polynomial is bounded in the interval $(-1, 1)$, the Hamiltonian is renormalized by shifting its eigenvalues to this range. Assuming the Fourier method for the spatial discretisation, the maximum energy represented on the grid is given by

$$E_{\max} = \frac{\hbar^2\pi^2}{2\mu(\Delta R)^2} + V_{\max}, \quad (13)$$

and the minimum energy $E_{\min} = V_{\min}$. Thus, the mean is

$$\bar{E} = \frac{1}{2}(E_{\max} + E_{\min}) \quad (14)$$

and the range

$$\Delta E = \frac{1}{2}(E_{\max} - E_{\min}). \quad (15)$$

Now, renormalizing the Hamiltonian by shifting its eigenvalues to $(-1, 1)$,

$$\hat{H}_{\text{norm}} = \frac{\hat{H} - \hat{I}\bar{E}}{\Delta E}, \quad (16)$$

and rewriting the evolution operator as

$$\exp\left(\frac{-i\hat{H}t}{\hbar}\right) = \exp\left(\frac{-i\bar{E}t}{\hbar}\right) \exp\left(\frac{-i\Delta E t \hat{H}_{\text{norm}}}{\hbar}\right), \quad (17)$$

and expanding it in a complex Chebychev series we get

$$\exp\left(\frac{-i\hat{H}t}{\hbar}\right) = \exp\left(\frac{-i\bar{E}t}{\hbar}\right) \sum_{n=0}^{\infty} C_n J_n(\alpha) T_n(-i\hat{H}_{\text{norm}}), \quad (18)$$

where $C_n = 1$ for $n=0$ and $C_n = 2$ for $n \geq 1$. The J_n 's are Bessel functions of the first kind of order n . $T_n(-i\hat{H}_{\text{norm}})$ are the

TABLE I. Grid parameters used for TDWP study.^a

Parameters	0°	90°	180°	Description
(R_{\min} , R_{\max})	(1.9,20.0)	(0.81,20.0)	(2.0,20.0)	Extension of grid along the R coordinate
ΔR	0.008 838	0.009 370	0.008 789	Grid spacing
N_R	2048	2048	2048	Number of grid points
E_{trans}/eV	9.5	9.5	9.5	Translational energy
δ	0.2	0.2	0.2	Width of the wavepacket
R_0	12.0	12.0	12.0	Initial location of the wavepacket
R_{mask}	15.0	15.0	15.0	R at which masking function is initiated
ΔR_{mask}	4.0	4.0	4.0	Width of the masking function
R_{max}	19.0	19.0	19.0	R at which WP becomes 0
t/fs	26.00	28.00	26.00	Total time WP is propagated

^aAll the quantities are in atomic units unless otherwise stated.

complex Chebychev polynomials satisfying the recurrence relation

$$\phi_{n+1} = -2i\hat{H}_{\text{norm}}\phi_n + \phi_{n-1}, \quad (19)$$

where

$$\phi_n = T_n(-i\hat{H}_{\text{norm}})\psi(0), \quad (20)$$

with the condition $\phi_0 = \psi(0)$ and $\phi_1 = -i\hat{H}_{\text{norm}}\psi(0)$. In this method the Bessel function $J_n(\alpha)$ with $\alpha = (\Delta E t / \hbar)$, falls off to zero exponentially for $n > \alpha$. This happens rapidly for larger α and for convergence 15 terms above $n = \alpha$ are included. A wavepacket is chosen with $\langle E_{\text{trans}} \rangle = 9.54$ eV for the time evolution. The width of the GWP is chosen as $0.2 a_0^{-1}$. The grid parameter used in the dynamics study is tabulated in the Table I. As the time evolves, because of coupling potential V_{12}^d , the WP starts partitioning to the excited PEC, ψ_2 , [CT channel, H(²S)+CO+(1² Σ^+)]. As the time is increased, there is continuous CT taking place between the two PECs. The evolving wavepacket hits the repulsive wall at small values of R and gets back. The dynamics of wavepacket propagation is studied for all the three molecular orientations namely for $\gamma = 0^\circ$, 90° , and 180° . The snap-shots of the time-evolution of the WP are displayed for $\gamma = 0^\circ$ in Fig. 7 as a representative example. The reflection of the WP from the grid edges at longer times is prevented by absorbing it near the edges with the use of absorbing boundaries. Here we have used \sin^2 damping function.⁵³ The damping function used is of the form

$$f(R_i) = \sin\left(\frac{\pi(R_{\text{mask}} + \Delta R_{\text{mask}} - R_i)}{2\Delta R_{\text{mask}}}\right), \quad (21)$$

where R_{mask} is the point at which the masking function is initiated and $\Delta R_{\text{mask}} (= R_{\text{max}} - R_{\text{mask}})$ is the width over which the function decays from 1 to 0 with the condition $\Delta R_{\text{mask}} \leq R_i$. We have used R_{mask} at 15.0 a_0 and $\Delta R_{\text{mask}} = 4.0 a_0$ for all the three molecular orientations. The probabilities for the total elastic (EC) and the CT channels are shown in Fig. 8 as a function of time for the three orientations. The probabilities have been obtained by integrating the evolving wavepacket on the ground and the first excited state PECs. One observes a greater population exchange of the flux for $\gamma = 90^\circ$ near 8 fs. This can be understood in terms of the NACME values (see Fig. 4) which show maximum modulus as compared to

other two orientations around $R = 8 a_0$. The overall average probability of the CT for the three orientations is $\approx 20\%$ as compared to that of the total elastic probability of $\approx 80\%$.

IV. FOUR-STATE COUPLING DYNAMICS

In this section we study the four-state coupling dynamics for the system. In Fig. 2(c) the $\gamma = 180^\circ$ approach shows that the avoided crossing regions are located further out in R and they are also found to be located at slightly lower values on the energy scale as compared to those observed for $\gamma = 0^\circ$ and 90° approaches. For $\gamma = 0^\circ$, ΔE between the asymptotic GS and the $4^1\Sigma^+$ state near the avoided crossing region at $R = 4.0 a_0$ is 8.81 eV, and for $\gamma = 180^\circ$, at $R = 4.8 a_0$ is 6.56 eV, respectively. ΔE between the asymptotic GS and the $4^1A'$ near the avoided crossing for $\gamma = 90^\circ$ at $R = 3.2 a_0$ is 6.71 eV. Different type of couplings exist between the PECs

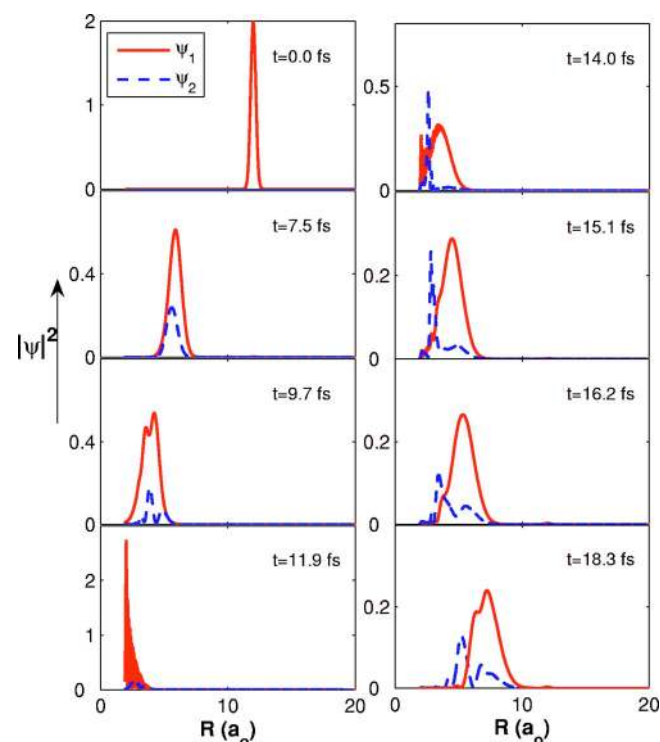


FIG. 7. Snap-shots of wavepacket propagating on two diabatic curves for 0° orientation. The wavepacket with dashed lines shows the time-evolution on the first excited state.

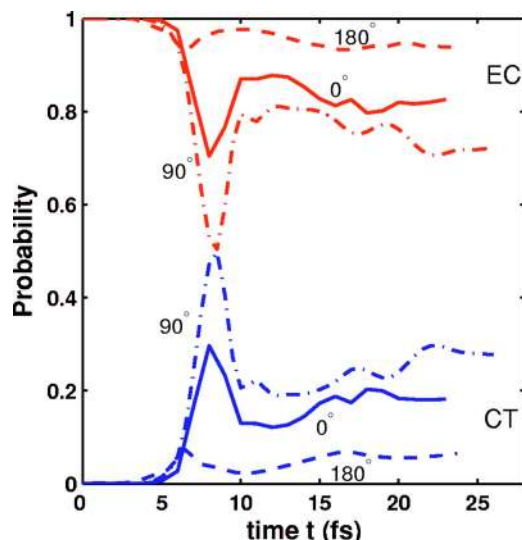


FIG. 8. Probability of the system at time t in the diabatic states. The sum of the two probabilities is one for all times.

for different ranges of R as illustrated in Fig. 2(c) for $\gamma = 180^\circ$. Rosen-Zener-Demkov type of coupling³⁶ exists between the GS and the first excited state PECs at larger radial distances whereas Landau-Zener type coupling³⁶ exist between the first and the second excited state PECs, and again between the second and the third excited state PECs at smaller radial distances. For $\gamma = 180^\circ$ and experimental collision energy $E_{\text{lab}} = 9.8$ eV ($E_{\text{trans}} = 9.5$ eV) the Landau-Zener type avoided crossing regions become accessible in addition to the Rosen-Zener-Demkov type of coupling between the GS and the first excited state. Therefore, we have examined the dynamics for this orientation involving all the four-states.

Using the MOLPRO code, NACME values have been computed simultaneously for the four-states, namely, τ_{12} , τ_{13} , τ_{14} , τ_{23} , τ_{24} , and τ_{34} and they are shown in Fig. 9. In the present case, the four-state diabatic coupling potential matrix is computed directly using the MOLPRO code in a similar way extending the two-state case and the diagonal elements (V_{11}^d ,

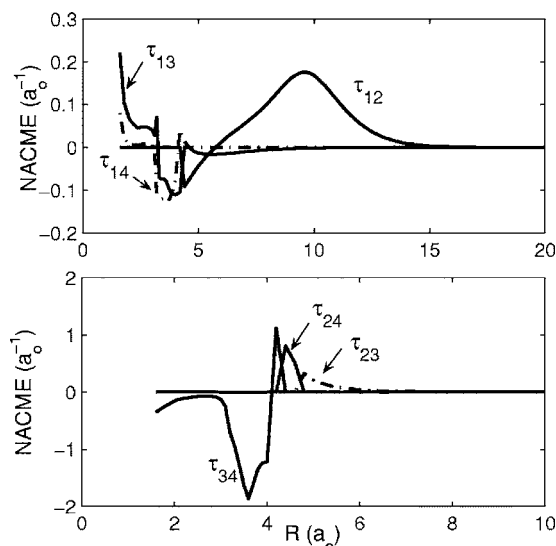


FIG. 9. Radial nonadiabatic coupling matrix elements (NACME) computed for the GS ($1^1\Sigma^+$) and the three excited states ($2-4^1\Sigma^+$) for $\gamma = 180^\circ$.

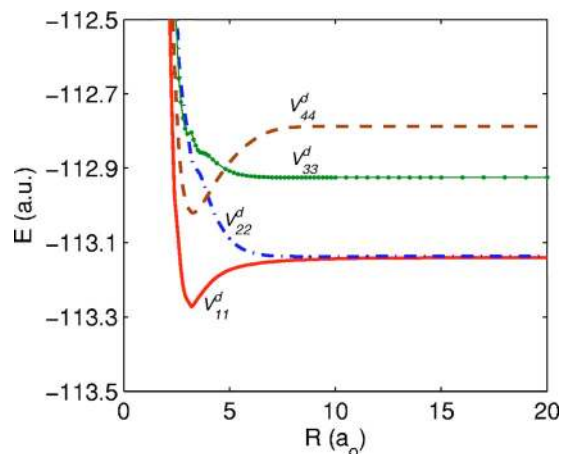


FIG. 10. Diabatic potential energy curves for $\gamma = 180^\circ$ orientation.

V_{22}^d , V_{33}^d , and V_{44}^d) are shown in the Fig. 10. Here, the diabatic PECs corresponding to the excited states show direct curve crossings for Landau-Zener type of coupling. It is worth pointing out here that Balint-Kurti *et al.* (see Ref. 41) have also recently computed the diabatic PECs corresponding to the five lowest adiabatic PECs in O_3 system using the MOLPRO code. However, one would like to note that a new diabaticization procedure has also been proposed by Vertesi *et al.*⁴³ just recently for N -state adiabatic-to-diabatic transformation where they have applied to three- to five-state *ab initio* calculations for the $\text{H} + \text{H}_2$ system.

The time-dependent Schrödinger equation for the nuclear motion in the diabatic representation is given as

$$i\hbar \frac{\partial}{\partial t} \begin{pmatrix} \psi_1(t) \\ \psi_2(t) \\ \psi_3(t) \\ \psi_4(t) \end{pmatrix} = \left[\begin{pmatrix} \hat{T}_1 & 0 & 0 & 0 \\ 0 & \hat{T}_2 & 0 & 0 \\ 0 & 0 & \hat{T}_3 & 0 \\ 0 & 0 & 0 & \hat{T}_4 \end{pmatrix} + \begin{pmatrix} V_{11}^d & V_{12}^d & V_{13}^d & V_{14}^d \\ V_{12}^d & V_{22}^d & V_{23}^d & V_{24}^d \\ V_{13}^d & V_{23}^d & V_{33}^d & V_{34}^d \\ V_{14}^d & V_{24}^d & V_{34}^d & V_{44}^d \end{pmatrix} \right] \begin{pmatrix} \psi_1(t) \\ \psi_2(t) \\ \psi_3(t) \\ \psi_4(t) \end{pmatrix}. \quad (22)$$

The TDWP dynamics is modeled on the diabatic PECs for this orientation using the same parameters defined in Table I with $\langle E_{\text{trans}} \rangle = 9.54$ eV. The initial WP, ψ_1 (shown in solid lines), is prepared in the asymptotic region on the V_{11}^d GS PEC corresponding to $\text{H}^+ + \text{CO}$ channel. As the time evolves, (see Fig. 11) because of coupling potential V_{12}^d at large radial distances, the WP starts partitioning on the V_{22}^d , the first excited state PEC, ψ_2 (shown in dashed lines). In the vicinity of the avoided crossing region, the WP again gets partitioned on the V_{33}^d , the second excited state PEC, ψ_3 , (shown in dashed-dotted lines). This portion of the WP gets stuck in the interaction region for a longer time even though components of the WP on the V_{11}^d and V_{22}^d get back in the asymptotic region after colliding with the repulsive regions. As the system ex-

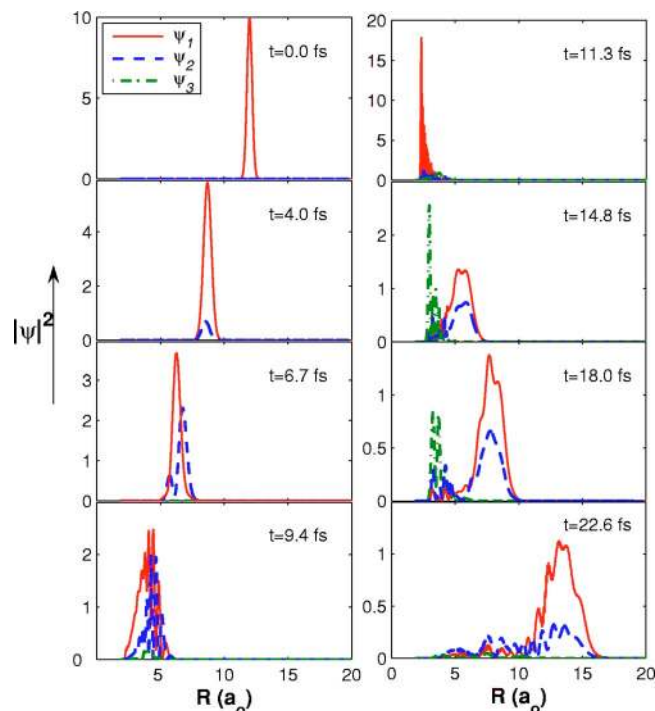


FIG. 11. Snap-shots of wavepacket propagating on four diabatic curves for 180° . See the text.

hibits long-time dynamics, the WP on the V_{11}^d and V_{22}^d reach the grid edges and reflect back. Hence the components of the WP are absorbed near the grid edge with the use of \sin^2 damping function [Eq. (21)].

The probabilities have been analyzed and they are shown in Fig. 12 as a function of time which show that the total elastic channel (EC) probability is around 68% whereas the first CT channel (CT_1) probability is of 30% and the remaining 2% is due to the second CT channel (CT_2) probability. A negligibly small portion of the WP evolves on the fourth PEC which is not included in Fig. 11 and the corresponding probability is not shown in Fig. 12. The overall CT probability have been found to be $\approx 32\%$. Since the probability for the second excited state CT channel (CT_2), [$H(2S) + CO^+(2^2\Sigma^+)$], is found to be small, this indirectly explains

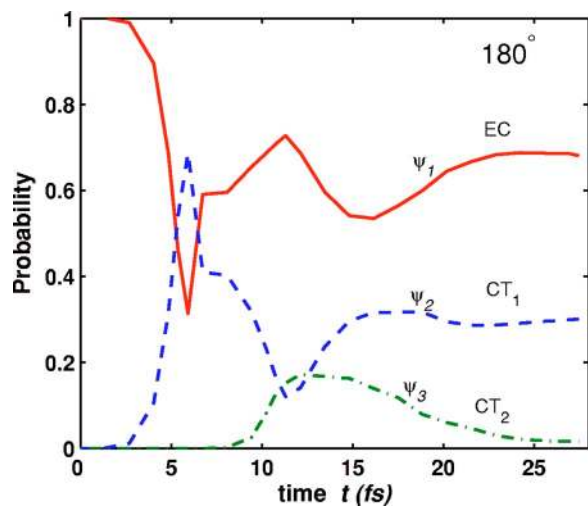


FIG. 12. Probability of the system at time t in the diabatic states.

why the proton energy-loss experiments did not observe any such CT collisions in the second excited state. It is important to point out here that the experiments were performed at $E_{\text{lab}}=30.0$ eV ($E_{\text{trans}}=28.96$ eV). A full three-dimensional quantum dynamics study for the collision energy $E_{\text{trans}}=9.5-30.0$ eV is currently under investigation.

V. SUMMARY AND CONCLUSIONS

In the present study *ab initio* PECs for the GS and the low-lying excited states have been obtained by the MRCI method employing the *cc-pVTZ* basis for the three different molecular orientations namely, H^+ approaching the O-end and C-end (collinear) and H^+ approaching the CO molecule in the perpendicular configuration with the CO distance fixed at its equilibrium value. The GS and the first excited states of all the three orientations show a Rosen-Zener-Demkov type of coupling in the asymptotic region whereas the first and the second excited states, and the second and the third excited states show Landau-Zener type of coupling with avoided crossings. Using the MOLPRO code, NACME values have been computed for the two-states involving the GS and the first excited states, and for the four-states involving the GS and the three lowest excited states of $1^1\Sigma^+$ symmetry. The diabatic coupling potential matrix for the two-state and the four-state couplings have been obtained directly from the MOLPRO code.

The quantum dynamics of the total elastic and the charge transfer collisions have been modeled with the two-state and four-state couplings. The TDWP dynamics is studied for the two-state coupling using the diabatic potentials at $\langle E_{\text{trans}} \rangle = 9.54$ eV for all the three orientations. The TDWP study is also carried out for the four-state coupling using the corresponding diabatic potentials for $\gamma=180^\circ$ orientation at $\langle E_{\text{trans}} \rangle = 9.54$ eV. The total elastic and charge transfer probabilities have been computed in both dynamics study. The CT probability in the two-state coupling dynamics for $\gamma = 180^\circ$ is found to be $\approx 10\%$ whereas in the four-state coupling dynamics it is found to be $\approx 30\%$ for the first CT channel, and $\approx 2\%$ for the second CT channel. Overall, the CT probability is small as compared to the total elastic channel probability which is in qualitative agreement with the experimental findings.

ACKNOWLEDGMENTS

This study was supported by a grant from the Department of Science and Technology, New Delhi under a fast track scheme. T.J.D.K. acknowledges the CSIR, New Delhi for Research Fellowship. The financial assistance by IIT Madras in procuring the MOLPRO code through the interdisciplinary research program in the chemical physics is also gratefully acknowledged.

¹W. Klemperer, *Nature (London)* **227**, 1230 (1970).

²H. Udseth, C. F. Giese, and W. R. Gentry, *J. Chem. Phys.* **60**, 3051 (1974).

³J. Krutein and F. Linder, *J. Chem. Phys.* **71**, 599 (1979).

⁴G. Niedner-Schatteburg and J. P. Toennies, *Adv. Chem. Phys.* **LXXXII**, 553 (1992).

⁵G. Niedner-Schatteburg, Dissertation, Georg-August-Universität Göttingen, Fachbereich Physik, 1988; also published as Bericht **13/1988**,

- Max-Planck-Institut für Strömungsforschung, Göttingen, 1988.
- ⁶F. A. Gianturco, *The transfer of molecular energies by collisions* (Springer, Berlin, 1979).
- ⁷E. Herbst, Chem. Soc. Rev. **30**, 168 (2001).
- ⁸M. Noll, Dissertation, Georg-August-Universität Göttingen, Fachbereich Physik, 1986; also published as Bericht **8/1986**, Max-Planck-Institut für Strömungsforschung, Göttingen, 1986.
- ⁹F. A. Gianturco, S. Kumar, and F. Schneider, Chem. Phys. **211**, 33 (1996); F. A. Gianturco, S. Kumar, T. Ritschel, R. Vetter, and L. Züllicke, J. Chem. Phys. **107**, 6634 (1997).
- ¹⁰R. Schinke and P. McGuire, Chem. Phys. **31**, 391 (1978); G. Parker and R. T. Pack, J. Chem. Phys. **72**, 1585 (1978).
- ¹¹R. Schinke, J. Chem. Phys. **72**, 3916 (1980); M. Baer, G. Niedner-Schatteburg, and J. P. Toennies, *ibid.* **91**, 4196 (1989); F. A. Gianturco and S. Kumar, Chem. Phys. **196**, 485 (1995); F. A. Gianturco and S. Kumar, J. Chem. Phys. **103**, 2940 (1995).
- ¹²F. A. Gianturco, A. Palma, E. Semprini, F. Stefani, and M. Baer, Phys. Rev. A **42**, 3926 (1990).
- ¹³I. Last, M. Gilibert, and M. Baer, J. Chem. Phys. **107**, 1451 (1997).
- ¹⁴T. Takayanagi, Y. Kurosaki, and A. Ichihara, J. Chem. Phys. **112**, 2615 (2000).
- ¹⁵V. G. Ushakov, K. Nobusada, and V. I. Osherov, Phys. Chem. Chem. Phys. **3**, 63 (2001).
- ¹⁶T. J. Dhillip Kumar and Sanjay Kumar, J. Chem. Phys. **121**, 191 (2004).
- ¹⁷C. Puzzarini, R. Tarroni, P. Palmieri, S. Carter, and L. Dore, Mol. Phys. **87**, 879 (1996).
- ¹⁸M. Mladenovic and S. Schmatz, J. Chem. Phys. **109**, 4456 (1998).
- ¹⁹N. Rosen and C. Zener, Phys. Rev. **40**, 502 (1932); Y. N. Demkov, Sov. Phys. JETP **18**, 138 (1964).
- ²⁰M. Kimura, J. P. Gu, G. Hirsch, R. J. Buenker, and P. C. Stancil, Phys. Rev. A **61**, 032708 (2000).
- ²¹R. S. Gao, L. K. Johnson, C. L. Hakes, K. A. Smith, and R. F. Stebbings, Phys. Rev. A **41**, 5929 (1990).
- ²²MOLPRO is a package of *ab initio* programs written by H.-J. Werner, P. J. Knowles, M. Schütz *et al.*
- ²³T. H. Dunning, Jr., J. Chem. Phys. **90**, 1007 (1989).
- ²⁴M. Kimura and N. F. Lane, Adv. At., Mol., Opt. Phys. **26**, 79 (1989).
- ²⁵A. Mead and D. Truhlar, J. Chem. Phys. **77**, 6090 (1982).
- ²⁶H.-J. Werner and W. Meyer, J. Chem. Phys. **74**, 5802 (1981).
- ²⁷H.-J. Werner, B. Follmeg, and M. H. Alexander, J. Chem. Phys. **89**, 3139 (1988); H.-J. Werner, B. Follmeg, M. H. Alexander, and P. Lemoine, *ibid.* **91**, 5425 (1989).
- ²⁸B. Heumann, K. Weide, R. Duren, and R. Schinke, J. Chem. Phys. **98**, 5508 (1992), and references therein.
- ²⁹D. Simah, B. Hartke, and H.-J. Werner, J. Chem. Phys. **111**, 4523 (1999), and references therein.
- ³⁰F. T. Smith, Phys. Rev. **179**, 111 (1969).
- ³¹M. Baer, Adv. Chem. Phys. **124**, 39 (2002); M. Baer, Phys. Rep. **358**, 75 (2002); M. Baer, in *Theory of Chemical Reaction Dynamics*, edited by M. Baer (CRC, Boca Raton, FL, 1985), Chap. 4, Vol. II.
- ³²M. Baer, G. N. Schatteberg, and J. P. Toennies, J. Chem. Phys. **91**, 4169 (1989).
- ³³V. Sidis, Adv. Chem. Phys. **82**, 73 (1992).
- ³⁴T. Pacher, L. S. Cederbaum, and H. Köppel, Adv. Chem. Phys. **84**, 293 (1993).
- ³⁵R. Schinke, in *Photodissociation dynamics* (Cambridge University Press, Cambridge, 1993).
- ³⁶H. Nakamura, in *Dynamics of Molecules and Chemical Reactions*, edited by R. E. Wyatt and J. Z. H. Zhang (Marcel Dekker, New York, 1996).
- ³⁷M. S. Child, Adv. Chem. Phys. **124**, 1 (2002); S. Adhikari and G. D. Billing, *ibid.* **124**, 143 (2002); G. A. Worth and M. A. Robb, *ibid.* **124**, 355 (2002).
- ³⁸A. W. Jasper, C. Zhu, S. Nangia, and D. G. Truhlar, Faraday Discuss. **127**, 1 (2004); A. W. Jasper, M. D. Hack, and D. G. Truhlar, J. Chem. Phys. **115**, 1804 (2001).
- ³⁹H. Köppel, Faraday Discuss. **127**, 35 (2004).
- ⁴⁰M. Baer, T. Vertesi, G. J. Halasz, A. Vibok, and S. Suhai, Faraday Discuss. **127**, 337 (2004).
- ⁴¹General discussion, Faraday Discuss. **127**, 81 (2004).
- ⁴²P. Baragan, L. F. Errea, A. Macias, L. Mendez, I. Rabadan, A. Riera, J. M. Lucas, and A. Aguilar, J. Chem. Phys. **121**, 11629 (2004); T. Romero, A. Aguilar, and F. X. Gadea, *ibid.* **110**, 6219 (1999).
- ⁴³T. Vertesi, E. Bene, A. Vibok, G. J. Halasz, and M. Baer, J. Phys. Chem. A **109**, 3476 (2005), and references therein.
- ⁴⁴Z. H. Top and M. Baer, Chem. Phys. **25**, 1 (1977); M. Baer and J. A. Beswick, Phys. Rev. A **19**, 1559 (1979); M. Baer, in *Molecular Collision Dynamics*, edited by J. M. Bowman (Springer, Berlin, Heidelberg, 1983).
- ⁴⁵H. Köppel, W. Domcke, and L. S. Cederbaum, Adv. Chem. Phys. **57**, 59 (1984).
- ⁴⁶M. Desouter-Lecomte, D. Dehareng, and J. C. Lorquet, J. Chem. Phys. **86**, 1429 (1987).
- ⁴⁷T. Pacher, L. S. Cederbaum, and H. Köppel, J. Chem. Phys. **89**, 7367 (1988).
- ⁴⁸C. Petrongolo, G. Hirsch, and R. J. Buenker, Mol. Phys. **70**, 825 (1990); G. Hirsch, R. J. Buenker, and C. Petrongolo, *ibid.* **70**, 835 (1990).
- ⁴⁹N. Balakrishnan, C. Kalyanaraman, and N. Sathyamurthy, Phys. Rep. **280**, 79 (1997), and references therein.
- ⁵⁰V. Mohan and N. Sathyamurthy, Comput. Phys. Commun. **7**, 213 (1988).
- ⁵¹R. Kosloff, J. Phys. Chem. **92**, 2087 (1988).
- ⁵²H. Tal-Ezer and R. Kosloff, J. Chem. Phys. **81**, 3967 (1984).
- ⁵³B. Maiti, S. Mahapatra, and N. Sathyamurthy, J. Chem. Phys. **113**, 59 (2000).